

MIX-DOMAIN CONTRASTIVE LEARNING FOR UNPAIRED H&E-TO-IHC STAIN TRANSLATION

Song Wang^{1,2}, Zhong Zhang², Huan Yan³, Ming Xu⁴, Guanghui Wang¹

¹ Toronto Metropolitan University, Toronto, M5B 2K3, Canada

² Zhengzhou University, Zhengzhou, 450001, China

³ The First Affiliated Hospital of Zhengzhou University, Zhengzhou, 450000, China

⁴ Zhongyuan University of Technology, Zhengzhou, 451191, China

ABSTRACT

H&E-to-IHC stain translation techniques offer a promising solution for precise cancer diagnosis, especially in low-resource regions where there is a shortage of health professionals and limited access to expensive equipment. Considering the pixel-level misalignment of H&E-IHC image pairs, current research explores the pathological consistency between patches from the same positions of the image pair. However, most of them overemphasize the correspondence between domains or patches, overlooking the side information provided by the non-corresponding objects. In this paper, we propose a Mix-Domain Contrastive Learning (MDCL) method to leverage the supervision information in unpaired H&E-to-IHC stain translation. Specifically, the proposed MDCL method aggregates the inter-domain and intra-domain pathology information by estimating the correlation between the anchor patch and all the patches from the matching images, encouraging the network to learn additional contrastive knowledge from mixed domains. With the mix-domain pathology information aggregation, MDCL enhances the pathological consistency between the corresponding patches and the component discrepancy of the patches from the different positions of the generated IHC image. Extensive experiments on two H&E-to-IHC stain translation datasets, namely MIST and BCI, demonstrate that the proposed method achieves state-of-the-art performance across multiple metrics.

Index Terms— Mix-domain contrastive learning, pathological consistency, component discrepancy, H&E-to-IHC stain translation.

1. INTRODUCTION

Hematoxylin and Eosin (H&E) staining is the most representative histochemical staining technique in the histopathological analysis workflow, enabling the visualization of distinct

tissue components in various colors, thereby facilitating cancer identification [1, 2, 3]. Due to its cost-effectiveness, H&E staining is widely utilized in cancer diagnosis [4]. However, relying solely on H&E staining images may not suffice for accurate differentiation of cancer subtypes by pathologists. To improve this limitation, Immunohistochemistry (IHC) staining techniques are developed to visualize specific antigens or proteins in the tissue via the interaction between labeled antibodies and intracellular antigens [5]. For example, Ki-67 IHC examination can stain positive tumor cells brown and negative ones blue, providing a selective and high-contrast visual result for pathologists to confirm the malignancy types [6]. Despite its high accuracy, IHC examination is labor-intensive and time-consuming, often requiring expensive equipment and advanced technologies. This poses a significant barrier to the widespread applications of pathology diagnostic services in low-income regions. Therefore, developing an effective and affordable method for IHC image acquisition is imperative.

To achieve this objective, researchers exploit data-driven approaches to transfer H&E-stained images to IHC-stained ones. However, an outstanding challenge faced by the approaches is how to build matching H&E-IHC image pairs. Since a slice can be only stained once, obtaining pixel-aligned H&E-IHC image pairs is physically infeasible. In this case, the second best choice is cutting the serial tissue sections from the same tissue block and staining them separately. The adjacent cuts stained by different methods are viewed as the matching H&E-IHC image pairs. Several matching H&E-IHC image pairs from available public datasets are shown in Fig. 1. It is obvious that these matching H&E-IHC image pairs are pixel-wise unpaired. For the unpaired matching images, there are some attempts to register them [3, 7, 8]. For example, Liu et al. [8] propose to register the matching H&E-IHC images at the structure level and obtain the structure-aligned H&E-IHC image pairs. However, those registration methods suffer from expert shortages and low efficiency.

An alternative solution is training the H&E-to-IHC translation model by directly utilizing the unpaired images. The

Corresponding Author: Guanghui Wang(wangcs@torontomu.ca).

This work was partly supported by the Natural Sciences and Engineering Research Council of Canada (NSERC).

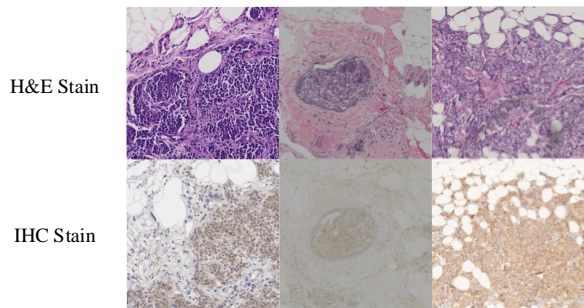


Fig. 1. Some examples of H&E-IHC image pairs from public MIST [9] and BCI [8] datasets. Matching H&E-IHC images are unpaired at the pixel level.

most representative H&E-to-IHC translation methods are the CycleGan-based ones [3, 10, 11, 12, 13], where the inverse generation process ensures the structure consistency between the generated image and the source image. However, these approaches hardly generate virtual IHC images with the same pathological properties as input H&E images. To address this issue, patch-wise contrastive learning is introduced into H&E-to-IHC stain translation. Li et al. [9] build a contrastive learning translation framework to maintain the pathological consistency between the corresponding patches from different images by mapping them together in embedding spaces.

The implicit hypothesis behind patch-wise contrastive learning is that the corresponding patches from matching images should have the same probability of cancer diagnosis. Based on this hypothesis, patch-wise contrastive learning has shown promising achievements in unpaired image-to-image translation tasks. However, the patch-wise contrastive learning method overemphasizes the contribution of the patches from the inter-domain (Fig. 2(a)), ignoring the patches from the intra-domain (Fig. 2(b)). Since the cancer cells distribute randomly in the tissue, as the brown cells in the IHC images from Fig. 1, we argue that the patches from the intra-domain typically have a different probability of cancer diagnosis but a similar appearance with the anchor, which provides excellent hard negatives for the contrastive learning. By collecting the patches from the intra-domain as negatives, the generation network is enforced to focus on the subtle differences between the patches from the same domain, further generating the virtual IHC-stained images with discriminative component details.

In this paper, we propose a Mix-Domain Contrastive Learning (MDCL) method for unpaired H&E-to-IHC stain translation. Specifically, MDCL method estimates the correlation between the anchor patch and all the patches from both inter- and intra-domains. This distinctive feature encourages the network to acquire additional contrastive knowledge from both staining domains and generate the virtual IHC-stained

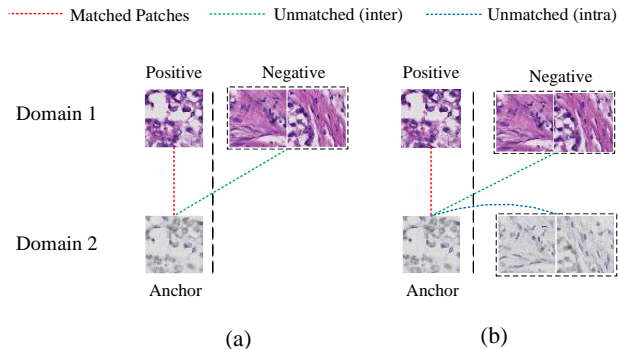


Fig. 2. The difference between (a) existing methods and (b) MDCL. For each anchor patch, existing methods only consider inter-domain patches (red and green). MDCL utilizes patches from both inter- (red and green) and intra-domain (blue).

images with discriminative local details.

The main contributions of this paper include:

- MDCL is proposed for the unpaired translation of H&E to IHC stains. MDCL combines inter-domain and intra-domain pathology information to improve pathological consistency between the input-generated image pairs and the component discrepancies in patches from different positions of the generated IHC image.
- Extensive experimental evaluations on two H&E-to-IHC stain translation datasets, MIST and BCI, demonstrate that the proposed method achieves state-of-the-art performance. Visualization results further illustrate MDCL’s superiority in preserving component details.

2. METHODS

In this section, we first present the H&E-to-IHC stain translation framework based on patch-wise contrastive learning. Then, we provide a detailed presentation of the mix-domain contrastive learning method in Sec. 2.2.

2.1. H&E-to-IHC Stain Translation Learning

Fig. 3 illustrates the proposed H&E-to-IHC stain translation learning framework. Given the input H&E stained image I_{he} , its corresponding virtual IHC stained image I_{ihc}^v is generated by the generator G of GAN. The discriminator D is utilized to distinguish whether the virtual IHC stained image I_{ihc}^v is similar to the real one I_{ihc}^{gt} . For the generated I_{ihc}^v , M patches are randomly sampled to construct the anchor set $A = \{a_1, a_2, \dots, a_M\}$. Meanwhile, the patches at the same locations are selected from the input H&E image I_{he} as the positive set $P^{he} = \{p_1^{he}, p_2^{he}, \dots, p_M^{he}\}$. For the matching pairs $(a_i, p_i^{he})_{i=1, \dots, M}$, a Siamese network f

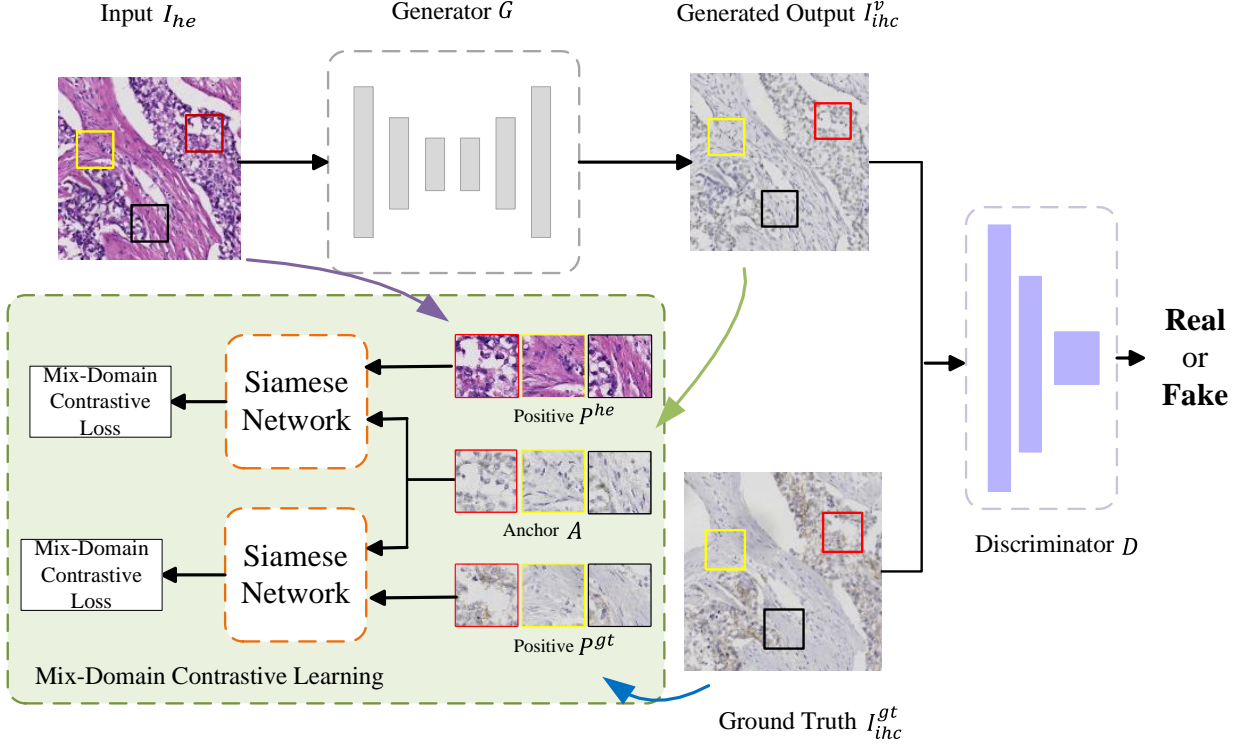


Fig. 3. H&E-to-IHC stain translation learning framework. Given the input H&E stained image I_{he} , the generator G generates the virtual IHC stained image I_{ihc}^v . M patches from I_{ihc}^v are randomly sampled to construct the anchor set A . At the same locations, the positive patches p_i^{he} from I_{he} and p_i^{gt} from I_{ihc}^{gt} are selected to build P^{he} and P^{gt} . The Siamese network f maps each pair of (a_i, p_i) together under the constraint of the mix-domain contrastive loss.

is built to map the matching patches together under the constraint of the contrastive loss. To exploit the supervised information from the ground-truth I_{ihc}^{gt} , a pixel-misaligned positive set $P^{gt} = \{p_1^{gt}, p_2^{gt}, \dots, p_M^{gt}\}$ is constructed, where p_i^{gt} is the corresponding patch to the anchor a_i . Similar to p_i^{he} , p_i^{gt} is also demanded to be closer to a_i in the embedding space. To relieve the misalignment problem at the pixel level, the adaptive weighting scheme from [9] is adopted to control the influence of patch pairs on the loss value.

2.2. Mix-Domain Contrastive Learning

Contrastive learning aims to pull the positive patch pairs closer and push the negative patch pairs apart in the embedding space. We take the input-generated image pair as an example in the following explanation. For each virtual IHC patch a_i , its embedding is denoted as $z_i = f(a_i)$. Similarly, the embedding of the corresponding H&E patch p_i^{he} can be represented as $z_i^{he} = f(p_i^{he})$. It is important to note that the last layer of the Siamese network f is typically a L_2 Normalization layer, allowing the patches to be mapped onto a unit hypersphere.

For the anchor set A and its positive set P^{he} , the proba-

bility of a_i matching with p_i^{he} can be represented as

$$\mathcal{P}_i^{he} = \frac{\exp(z_i \cdot z_i^{he} / \tau)}{\exp(z_i \cdot z_i^{he} / \tau) + \sum_{j=1, j \neq i}^M \exp(z_i \cdot z_j^{he} / \tau)}, \quad (1)$$

where τ stands for the temperature which controls the concentration level of the class distribution [14]. In Eq.(1), z_i^{he} denotes the positive embedding of the anchor z_i , while $z_{j \neq i}^{he}$ represents the negative embedding. Since z is on the unit hypersphere, the dot product of z_i and z_j^{he} stands for the cosine similarity between the anchor patch from IHC domain and the j -th patch from H&E domain. The ratio of $z_i \cdot z_i^{he}$ to $\sum_{j=1}^M z_i \cdot z_j^{he}$ indicates the probability of a_i matching with p_i^{he} . The original patch-based contrastive loss [15] is designed as the negative log-likelihood of the probability \mathcal{P}_i

$$\mathcal{L}_i = -\log \left[\frac{\exp(z_i \cdot z_i^{he} / \tau)}{\exp(z_i \cdot z_i^{he} / \tau) + \sum_{j=1, j \neq i}^M \exp(z_i \cdot z_j^{he} / \tau)} \right]. \quad (2)$$

Minimizing Eq.(2) can be viewed as maximizing the probability of a_i matching with p_i^{he} .

It is observed that the existing patch-based contrastive loss in Eq.(2) only considers the relationship between the anchor and the patches from different domains, like Fig. 2(a).

Following the implicit hypothesis behind patch-wise contrastive learning, it is well-known that the non-corresponding patches have different probabilities of cancer diagnosis. This hypothesis inspires us that the patches from the same domain with the anchor can also be viewed as negative patches, like Fig.2(b). In this case, the mix-domain contrastive loss for anchor a_i can be formulated as

$$\mathcal{L}_i^{he} = -\log \left[\frac{\exp(z_i \cdot z_i^{he}/\tau)}{\sum_{j=1}^M \exp(z_i \cdot z_j^{he}/\tau) + \sum_{j=1, j \neq i}^M \exp(z_i \cdot z_j/\tau)} \right], \quad (3)$$

where the first item in the denominator represents the inter-domain similarity while the intra-domain correlation is explored by the second item. The symbol z_j denotes the embedding of the negative patch from the same domain. By introducing negative patches with similar colors and appearances, the mix-domain contrastive loss aims at discriminating the subtle difference between the patches from the same domain, which in turn encourages the generator G to pay more attention to detail generation. The mix-domain contrastive loss for the anchor set A and the positive set P^{he} is written as follows

$$L_{mix}^{he} = \sum_{i=1}^M \mathcal{L}_i^{he}. \quad (4)$$

The whole learning process is illustrated in Fig.4. For the anchor set A and positive set P^{he} . All the patches from A and P^{he} are mapped onto the unit hypersphere by the Siamese network. For each anchor patch a_i , the mix-domain contrastive loss demands it to be close to the positive patch p_i^{he} and far away from all the rest of the patches on the unit hypersphere.

Similarly, the mix-domain contrastive loss for the anchor set A and the positive set P^{gt} is formulated as

$$L_{mix}^{gt} = \sum_{i=1}^M \omega_i \mathcal{L}_i^{gt}, \quad (5)$$

where ω_i means the adaptive weight [9] for the contrastive loss generated by the anchor a_i . In Eq.5, the groundtruth image and the generated IHC image are viewed as different domains.

To sum up, the overall learning objective for the generator G is defined as

$$L_{overall} = L_{adv} + L_{mix}^{he} + L_{mix}^{gt} + \lambda_{GP} L_{GP}, \quad (6)$$

where L_{adv} stands for the standard adversarial loss generated by the generator whereas L_{GP} represents the Gaussian Pyramid-based reconstruction loss [8]. The coefficient λ_{GP} is utilized to balance the contributions of L_{GP} to the generator training.

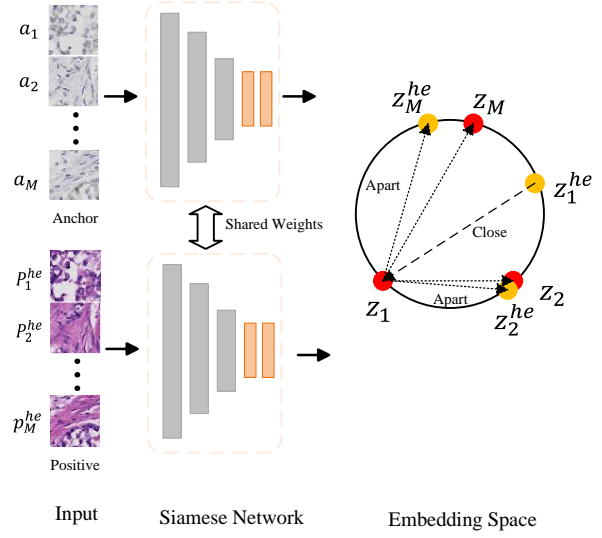


Fig. 4. Mix-domain contrastive learning for the anchor set A and positive set P^{he} . All the patches from A and P^{he} are at first mapped onto the unit hypersphere by the Siamese network. For each anchor a_i , its embedding z_i is demanded to be close to z_i^{he} (the embedding of the positive p_i^{he}) and far away from all the rest.

3. EXPERIMENTS

3.1. Datasets

MIST. The Multi-IHC Stain Translation dataset [9] consists of four subsets with different IHC stain approaches, namely HER2, ER, Ki67, and PR. For each subset, there are more than 4,000 image pairs for training and 1,000 image pairs for testing. The resolution of all images is 1024×1024 .

BCI. The Breast Cancer Immunohistochemical dataset [8] includes 4,873 H&E-IHC image pairs where 3,896 pairs are selected as training set and the rest 977 pairs as testing set by following the default setting¹. The IHC-stained images have four HER2 expression statuses: IHC 0, IHC 1+, IHC 2+, and IHC 3+, standing for the different staining stages. All images in BCI are of size 1024×1024 .

3.2. Implementation Details

Following the setting of [9], ResNet-6Blocks [16] and PatchGAN [17] are employed to be the generator and discriminator, respectively. The Siamese network is composed of the encoder part of the generator, two MLP layers with a ReLU layer in the middle, and an L2 Normalization layer. During the training, the images are randomly cropped to be 512×512 . The training epoch is set to 40. The initial learning rate is 2×10^{-4} and decreases using linear decay after 30 epochs. The Adam optimizer [18] with $\beta_1 = 0.5$ and

¹<https://bupt-ai-cz.github.io/BCI/>

Table 1. Evaluation results on MIST. The best values are in bold. KID values are shown by multiplying 1000.

Subset	Method	FID↓	PHV _{T=0.01} ↓					KID↓
			layer1	layer2	layer3	layer4	average	
HER2	CycleGAN	240.3	0.5633	0.6346	0.4695	0.8871	0.6386	311.1
	CUT+ L_{GP}	66.8	0.5321	0.4826	0.3060	0.8323	0.5383	19.0
	Pix2Pix	137.3	0.5516	0.5070	0.3253	0.8511	0.5588	82.9
	PyramidP2P	104.0	0.4787	0.4524	0.3313	0.8423	0.5262	61.8
	ASP	51.4	0.4534	0.4150	0.2665	0.8174	0.4881	12.4
	MDCL	44.4	0.4371	0.3944	0.2518	0.8171	0.4751	7.5
ER2	CycleGAN	125.7	0.5175	0.5092	0.3710	0.8672	0.5662	95.1
	CUT+ L_{GP}	43.7	0.4531	0.4079	0.2725	0.8194	0.4882	8.7
	Pix2Pix	128.1	0.5818	0.5282	0.3700	0.8620	0.5855	79.0
	PyramidP2P	107.4	0.4767	0.4538	0.3757	0.8567	0.5407	84.2
	ASP	41.4	0.4336	0.4007	0.2649	0.8205	0.4799	5.8
	MDCL	34.9	0.4533	0.3969	0.2646	0.8238	0.4854	3.6
Ki67	CycleGAN	343.9	0.8274	0.8275	0.6081	0.9038	0.7917	317.9
	CUT+ L_{GP}	76.1	0.5426	0.4739	0.3160	0.8415	0.5435	43.5
	Pix2Pix	147.0	0.5468	0.4905	0.3415	0.8496	0.5571	142.4
	PyramidP2P	94.4	0.4533	0.4222	0.3360	0.8363	0.5120	78.0
	ASP	51.0	0.4472	0.4001	0.2701	0.8128	0.4826	19.1
	MDCL	30.8	0.4005	0.3638	0.2465	0.8064	0.4543	6.1
PR	CycleGAN	96.1	0.5334	0.5554	0.3867	0.8654	0.5852	96.6
	CUT+ L_{GP}	54.6	0.4656	0.4128	0.2724	0.8154	0.4916	20.1
	Pix2Pix	183.8	0.6027	0.5569	0.4043	0.8601	0.6060	148.1
	PyramidP2P	98.8	0.5078	0.4682	0.3509	0.8446	0.5429	59.5
	ASP	44.8	0.4484	0.3898	0.2564	0.8080	0.4757	10.2
	MDCL	38.3	0.4320	0.3768	0.2499	0.8052	0.4660	7.1

$\beta_2 = 0.999$ is utilized for training. For the overall loss in Eq.(6), the coefficient λ_{GP} is set to 10, same as in [9]. The “lambda.linear” scheme is chosen in Eq.(5) to weight the pixel-misaligned patches. For each image pair, 256 patches are randomly selected to generate the anchor and positive sets.

Multiple metrics are employed to measure the performance of the proposed method. At first, this paper employs Fréchet Inception Distance (FID) [19] to compare the distributions of generated and groundtruth IHC images in the InceptionV3 feature space. By relaxing the Gaussian assumption in FID, Kernel Inception Distance (KID) [20] measures the squared Maximum Mean Discrepancy (MMD) between the Inception representations of the generated and groundtruth images. Additionally, Perceptual Hash Value (PHV) [12] is employed to gauge the content similarity of the generated and groundtruth pairs. In all the aforementioned metrics, a lower value means a better performance.

3.3. Experiment on MIST

Evaluation Results. We compared the proposed method with the existing image-to-image translation methods which include CycleGAN [21], CUT [15], Pix2Pix [17], PyramidP2P [8], ASP [9]. The quantitative results are shown in Table 1. We can see from the results that the lowest FID and

KID are achieved by MDCL on all the subsets, demonstrating the superiority of MDCL on different H&E-IHC translation tasks. Moreover, MDCL obtains the best PHV on most subsets, except for ER2 subset where the performance of MDCL is slightly worse than ASP.

Ablation Study. To verify the effectiveness of MDCL, this paper performs an ablation study and compares it with the original patch-based contrastive loss. The results on HER2 subset are presented in Table 2. We first evaluate the influence of MDCL only on the generated-input patch pair loss L^{he} . From the first two rows of Table 2, we can see that MDCL improves the H&E-to-IHC translation performance across all three metrics. We also assess the effect of MDCL on the combination of L^{he} and L^{gt} , where L^{gt} denotes the patch-based contrastive loss for generated-real IHC pairs. By replacing L^{he} and L^{gt} with L_{mix}^{he} and L_{mix}^{gt} , the proposed method brings significant performance gains on FID, PHV, and KID, demonstrating the effectiveness of MDCL.

Visualization Results. Some visual comparison results are illustrated in Fig.5. Fig.5 (a) shows the images with the original size. To highlight the visual effect of the generated IHC images, we crop the local patches in the red boxes and list them as (b) Input H&E, (c) GT IHC, (d) ASP, and (e) MDCL. Compared with the baseline ASP, MDCL generates the translation

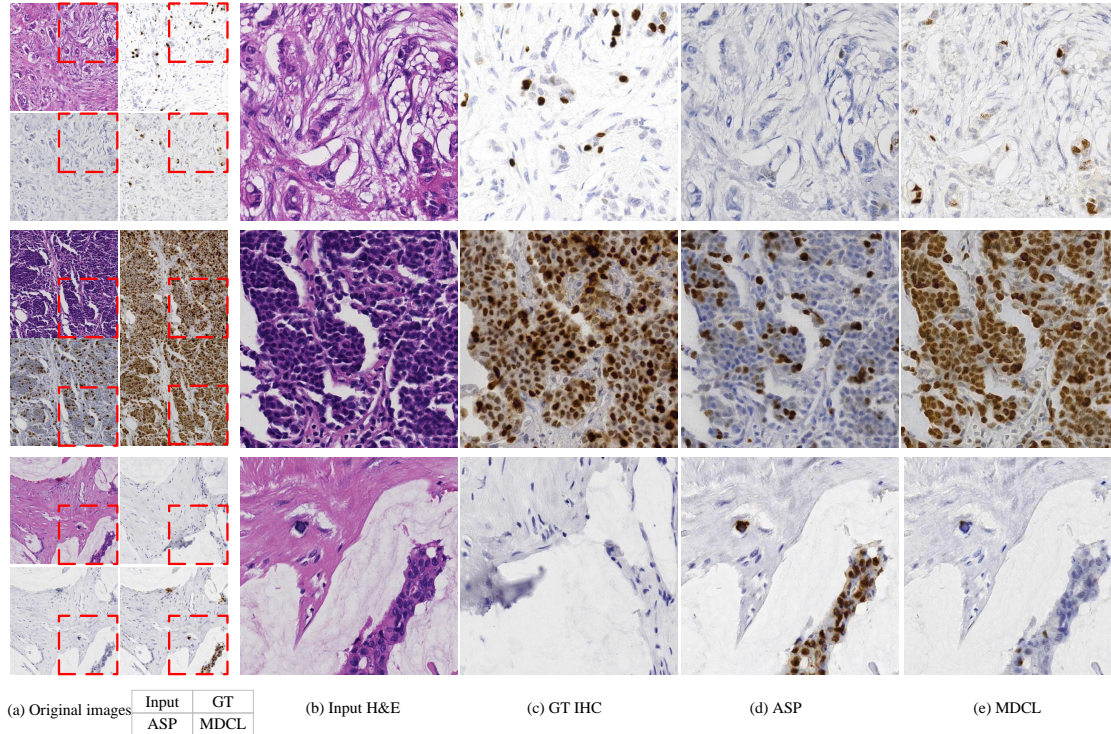


Fig. 5. Visualization results of some H&E-IHC image pairs. (a) Original images, including input H&E images, GroundTruth IHC images, and the generated IHC images with ASP and MDCL. (b) Input H&E patch, (c) Groundtruth IHC patch, (d) Generated IHC patch with ASP, (e) Generated IHC patch with MDCL.

Table 2. The ablation study on HER2 by replacing the original patch-based contrastive loss with MDCL. KID values are shown by multiplying 1000.

Method	FID↓	PHV $_{T=0.01}$ ↓ avg.(layer1~4)	KID↓
L^{he}	62.5	0.4997	26.9
L^{he}_{mix}	59.4	0.4960	21.1
$L^{he} + L^{gt}$	51.4	0.4881	12.4
$L^{he}_{mix} + L^{gt}_{mix}$	44.4	0.4751	7.5

results with more discriminative component details. For example, in the first two rows of Fig.5, the positive tumor cells (brown) are accurately translated by MDCL whereas the virtual IHC images generated by ASP contain rare positive tumor cells. When translating the negative tumor cells into the IHC domain (the last row), ASP generates incorrect staining results. Meanwhile, the generated IHC image with MDCL has an extreme similarity with the groundtruth.

3.4. Experiment on BCI

The superiority of the proposed method is also validated on BCI dataset. Since the training and testing sets in [9] are different from the default ones, we retrained the ASP model

Table 3. Evaluation results on BCI. KID values are shown by multiplying 1000. The symbol * means that we retrain the model on the default training set from BCI.

Method	FID↓	PHV $_{T=0.01}$ ↓				KID↓
		layer1	layer2	layer3	layer4	
ASP*	219.4	0.6436	0.5761	0.3860	0.8297	95.5
MDCL	51.2	0.4962	0.3861	0.2351	0.7344	13.0

to make a fair comparison with our method. The evaluation results on BCI are illustrated in Table 3. It is evident that our model achieves the best performance gains on all metrics, demonstrating the robustness of the proposed MDCL method.

4. CONCLUSION

In this paper, we have proposed the mix-domain contrastive learning for unpaired H&E-to-IHC stain translation. The proposed method treats matching images as different domains, and formulates a mix-domain contrastive loss, accounting for the impact of negative patches from both inter- and intra-domain on pathological consistency learning. Experimental results demonstrate that the proposed method achieves state-of-the-art performance on two publicly available H&E-to-IHC translation datasets.

5. REFERENCES

- [1] Aïcha BenTaieb and Ghassan Hamarneh, “Adversarial stain transfer for histopathology image analysis,” *IEEE transactions on medical imaging*, vol. 37, no. 3, pp. 792–802, 2017.
- [2] Yiyang Lin, Bowei Zeng, Yifeng Wang, et al., “Unpaired multi-domain stain transfer for kidney histopathological images,” in *Proceedings of the AAAI Conference on Artificial Intelligence*, 2022, vol. 36, pp. 1630–1637.
- [3] Bowei Zeng, Yiyang Lin, Yifeng Wang, et al., “Semi-supervised pr virtual staining for breast histopathological images,” in *International Conference on Medical Image Computing and Computer-Assisted Intervention*. Springer, 2022.
- [4] Jia-Mei Chen, Yan Li, Jun Xu, Lei Gong, Lin-Wei Wang, Wen-Lou Liu, and Juan Liu, “Computer-aided prognosis on breast cancer with hematoxylin and eosin histopathology images: A review,” *Tumor Biology*, vol. 39, no. 3, 2017.
- [5] Jose A Ramos-Vara, “Technical aspects of immunohistochemistry,” *Veterinary pathology*, vol. 42, no. 4, 2005.
- [6] Rafiq A Sheikh, Byung Hee Min, Shagufta Yasmeen, et al., “Correlation of ki-67, p53, and adnab-9 immunohistochemical staining and ploidy with clinical and histopathologic features of severely dysplastic colorectal adenomas,” *Digestive diseases and sciences*, vol. 48, pp. 223–229, 2003.
- [7] Yiqing Liu, Xi Li, Aiping Zheng, Xihan Zhu, et al., “Predict ki-67 positive cells in h&e-stained images using deep learning independently from ihc-stained images,” *Frontiers in Molecular Biosciences*, vol. 7, pp. 183, 2020.
- [8] Shengjie Liu, Chuang Zhu, Feng Xu, et al., “Bci: Breast cancer immunohistochemical image generation through pyramid pix2pix,” in *Proceedings of the IEEE/CVF Conference on Computer Vision and Pattern Recognition*, 2022, pp. 1815–1824.
- [9] Fangda Li, Zhiqiang Hu, Wen Chen, and Avinash Kak, “Adaptive supervised patchnce loss for learning h&e-to-ihc stain translation with inconsistent groundtruth image pairs,” in *International Conference on Medical Image Computing and Computer-Assisted Intervention*. Springer, 2023, pp. 632–641.
- [10] Wenju Xu and Guanghui Wang, “A domain gap aware generative adversarial network for multi-domain image translation,” *IEEE Transactions on Image Processing*, vol. 31, pp. 72–84, 2021.
- [11] Tianxiao Zhang, Wenchi Ma, and Guanghui Wang, “Six-channel image representation for cross-domain object detection,” in *Image and Graphics: 11th International Conference, ICIG 2021, Proceedings*. Springer, 2021, pp. 171–184.
- [12] Shuting Liu, Baochang Zhang, Yiqing Liu, et al., “Unpaired stain transfer using pathology-consistent constrained generative adversarial networks,” *IEEE Transactions on Medical Imaging*, vol. 40, no. 8, pp. 1977–1989, 2021.
- [13] Wenju Xu, Chengjiang Long, et al., “Drb-gan: A dynamic resblock generative adversarial network for artistic style transfer,” in *Proceedings of the IEEE/CVF international conference on computer vision*, 2021, pp. 6383–6392.
- [14] Zhirong Wu, Yuanjun Xiong, Stella X Yu, and Dahua Lin, “Unsupervised feature learning via non-parametric instance discrimination,” in *Proceedings of the IEEE conference on computer vision and pattern recognition*, 2018.
- [15] Taesung Park, Alexei A Efros, Richard Zhang, and Jun-Yan Zhu, “Contrastive learning for unpaired image-to-image translation,” in *Computer Vision—ECCV 2020: 16th European Conference, 2020, Proceedings*. Springer, 2020, pp. 319–345.
- [16] Justin Johnson, Alexandre Alahi, and Li Fei-Fei, “Perceptual losses for real-time style transfer and super-resolution,” in *14th European Conference, Proceedings, Part II 14*. Springer, 2016, pp. 694–711.
- [17] Phillip Isola, Jun-Yan Zhu, Tinghui Zhou, and Alexei A Efros, “Image-to-image translation with conditional adversarial networks,” in *Proceedings of the IEEE conference on computer vision and pattern recognition*, 2017, pp. 1125–1134.
- [18] Diederik P Kingma and Jimmy Ba, “Adam: A method for stochastic optimization,” in *International Conference on Learning Representations*, 2015.
- [19] Martin Heusel, Hubert Ramsauer, et al., “Gans trained by a two time-scale update rule converge to a local nash equilibrium,” *Advances in neural information processing systems*, vol. 30, 2017.
- [20] Mikołaj Bińkowski, Danica J Sutherland, Michael Arbel, and Arthur Gretton, “Demystifying mmd gans,” *arXiv preprint arXiv:1801.01401*, 2018.
- [21] Jun-Yan Zhu, Taesung Park, Phillip Isola, and Alexei A Efros, “Unpaired image-to-image translation using cycle-consistent adversarial networks,” in *Proceedings of the IEEE international conference on computer vision*, 2017.